

Multi-spectral programmable absorbers

Yun Meng¹, Dan Li¹, Chong Zhang³, Yang Wang³, Robert E. Simpson^{2*}, Yi Long^{1*}

¹ School of Materials Science and Engineering, Nanyang Technological University, 50 Nanyang Avenue, 639798, Singapore

² ACTA Lab, Singapore University of Technology and Design, 8 Somapah Road, 487372, Singapore

³ Shanghai Institute of Optics and Fine Mechanics, Chinese Academy of Sciences, Shanghai 201800, China

Corresponding author: robert_simpson@sutd.edu.sg and longyi@ntu.edu.sg

Abstract

We designed and demonstrated a multi-spectral programmable perfect absorber that exploits two different phase-change materials. This programmability is possible by resonantly coupling two phase change materials, a Ge₂Sb₂Te₅ layer to vanadium dioxide nanoparticles (VO₂ NPs). The perfect absorption is attributed to the coalescence of gap plasmon modes excited between the NPs and waveguide cavity-like modes excited between the film and the NPs. The absorptance peak (>90%) can be tuned to four different infrared (IR) wavelengths from 1906 to 2960 nm by heating the structure to different temperatures. The perfect absorber is reconfigurable, lithography-free, large-scale, polarization-insensitive omnidirectional. Our strategy opens a new path for programmable infrared photonics.

Corresponding author: robert_simpson@sutd.edu.sg; longyi@ntu.edu.sg

Perfect electromagnetic (EM) absorption has wide ranging applications, such as biosensing, display, photo-thermal conversion.¹⁻⁶ However, it is hard to achieve perfect absorption using natural materials due to the impedance-mismatch problem. Therefore, several plasmonic nanostructures and metasurfaces have been proposed to achieve high absorptance.⁷⁻¹¹ However, the optical response of these devices is usually fixed once the designed metasurface has been fabricated.

To enable tunable and reconfigurable perfect absorbers, there are essentially two options: (1) tune the geometry of the resonant cavity, or (2) tune the refractive index of the resonant cavity. Micro-electromechanical systems can be used to tune the cavity geometry, but this requires exquisite control of the micropatterning conditions and the devices can have cyclability issues.^{12,13} On the other hand, materials that exhibit a tunable refractive index, such as phase-change materials, graphene^{14,15} and liquid crystals¹⁶ are a viable solution. In particular, the phase change material, $\text{Ge}_2\text{Sb}_2\text{Te}_5$ (GST) incorporated metamaterials have shown promise for tuning of plasmon resonances. This tunability is attributed to plasmon resonances being sensitive to the refractive index (n) of the surroundings. Since the n of $\text{Ge}_2\text{Sb}_2\text{Te}_5$ can reversibly change from ~ 4 to ~ 6 in the IR between the amorphous state and crystalline states, using laser or electrical heat pulses¹⁷⁻¹⁹, it is particularly attractive for M-IR reprogrammable plasmonics.²⁰⁻²⁵

Patterning the nanoscale features of a metasurface usually requires expensive and time-consuming techniques, such as electron beam lithography. These points make electron beam lithography unattractive for mass fabrication on an industrial scale. In contrast, metallic nanoparticles (NPs) that exhibit local surface plasmon resonances (LSPRs) can

be manufactured at a low-cost synthesized.^{26,27} We propose, therefore, to couple these plasmonic phase change NPs with other phase change plasmonic structures to achieve electromagnetic resonances that can be tuned across a broadband.^{28,29} By combining multiple phase change materials, multiple resonant modes can be achieved.

In our previous work, we combined $\text{Ge}_2\text{Sb}_2\text{Te}_5$ and vanadium dioxide (VO_2) thin films to achieve a 2-bit, 4-state reflective switch. The switch allowed four different reflectivity levels for light with a wavelength of 680 nm.³⁰ We now extend this work by combining VO_2 nanoparticles (NPs) with a $\text{Ge}_2\text{Sb}_2\text{Te}_5$ thin film structure. VO_2 NPs undergo a metal-insulator-transition that changes the LSPRs wavelength.³¹⁻³⁴ We hypothesize that combining VO_2 NPs and $\text{Ge}_2\text{Sb}_2\text{Te}_5$ films can provide for different resonant wavelengths. We demonstrate a 4-state tunable resonant wavelength shift of a perfect absorber using self-assembled VO_2 NPs coupled to $\text{Ge}_2\text{Sb}_2\text{Te}_5$ thin films. The reversible change of the 4-state absorptance peaks allows perfect absorption programming from 1733 nm to 2888 nm. The LSPRs between the metals create a strong magnetic dipolar moment and thus achieve a high absorption. Furthermore, the strong absorptance is independent of the incident angle and the light's polarization state. The polarization-insensitive, large-scale, lithography-free and multi-level tunable functionality provides a fine modulation on the plasmonic resonant modes. This work lays the foundation for smart sensing, programmable modulators, reconfigurable optical switches, and more.

A schematic of the four-wavelength switch is shown in Figure 1(a). It consists of an 80 nm thick $\text{Ge}_2\text{Sb}_2\text{Te}_5$ layer, which was deposited on a silicon substrate by radio frequency

sputtering (AJA Orion5) from a $\text{Ge}_2\text{Sb}_2\text{Te}_5$ alloy target. A TiN layer, which was deposited using a Ti target by direct current magnetron sputtering in a reactive nitrogen atmosphere. The N_2 and Ar gases had the ratio 1:4. The Au film with a thickness of 90 nm was sputtered using a Au target with an RF power of 100 W. The chamber's background and sputtering pressure were 4×10^{-5} Pa and 0.2 Pa, respectively. The average particle size of VO_2 NPs (Ji-cheng, China) was 45 nm. The VO_2 NPs were dispersed in alcohol with the concentration of 2%. Then the VO_2 NPs solution was spin-coated onto the surface of the Au film.

The Finite-difference time-domain (FDTD, Lumerical) technique was used to solve Maxwell's equations and simulate the reflectance spectrum for different device design. In the model, the optical properties of VO_2 NPs and the $\text{Ge}_2\text{Sb}_2\text{Te}_5$ layer in Figs. 1e and 1f were used. The permittivity of TiN and Au were given by Philipp's data and Johnson and Christy's data.³⁵ The angular reflection of the absorber was measured using a spectroscopic ellipsometer for different incident angles varying from 20° to 80° . The absorptance was then calculated from $A=1-R-T$, where R and T are respectively the transmissivity and reflectivity. The size of VO_2 NPs was measured by transmission electron microscopy (TEM) in the bright field mode.

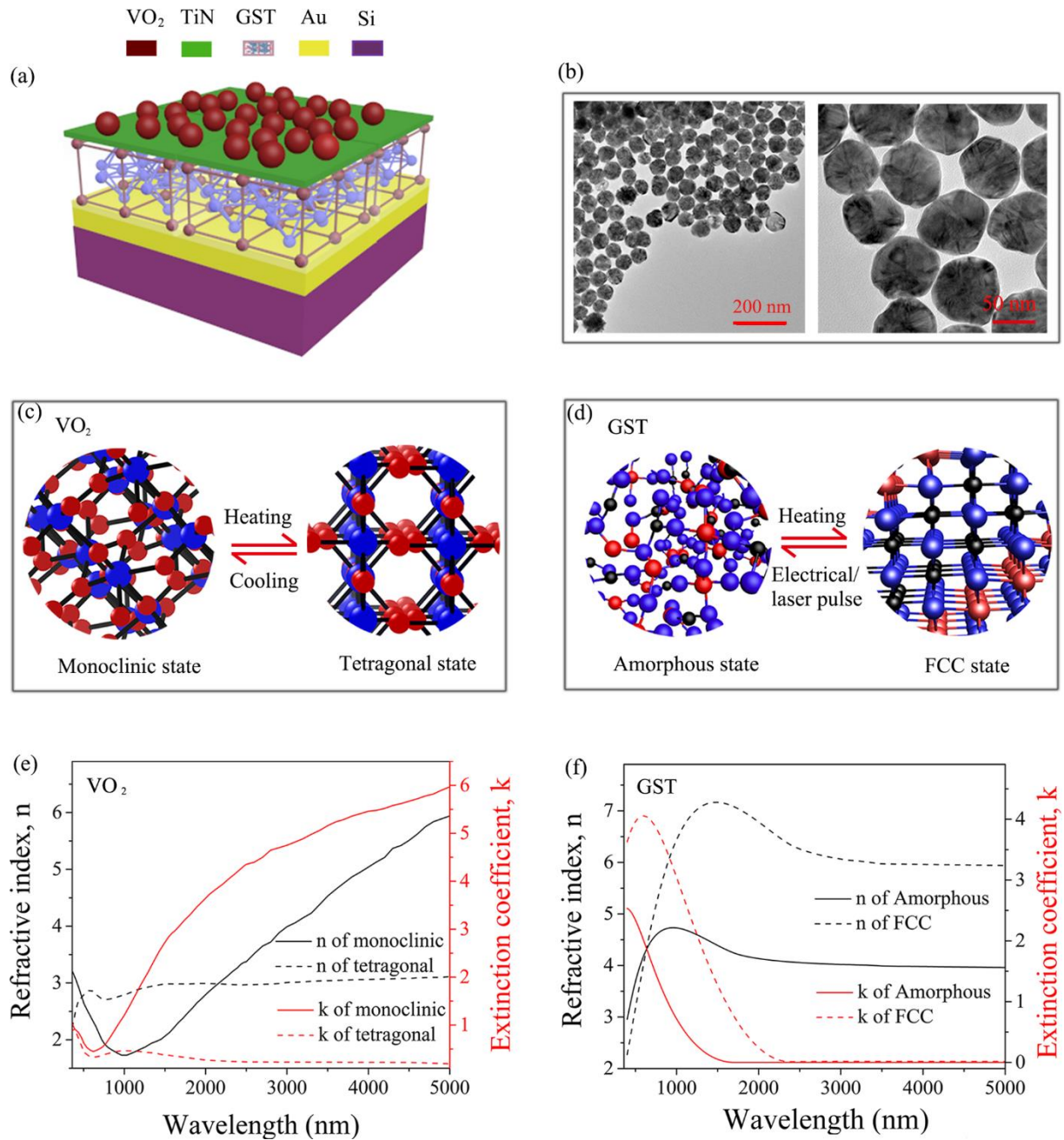


Figure 1 (a) Schematic of the reconfigurable absorber. The average diameter of VO₂ NPs is 90 nm. The thickness of TiN, GST and Au layer are 5 nm, 90 nm, and 80 nm, respectively. (b) TEM images of surface of the proposed absorber; (c) Schematic illustration of the reversible switching of VO₂ between monoclinic and tetragonal states; (d) Schematic illustration of the reversible switching of the GST between amorphous and Face Centered Cubic (FCC) states; The refractive index of (e) VO₂; (f) GST.

Fig. 1a illustrates the proposed reconfigurable absorber. An Au layer of 80 nm was firstly deposited on silicon (Si) substrate. The Au layer acts as a mirror to enhance the reflected signal, while also interacting with the top VO₂ NPs (tetragonal state) to create

displacement current loops, which leads to the strong magnetic dipolar resonance. A 5 nm TiN was sandwiched between the Ge₂Sb₂Te₅ and VO₂ NPs to protect the Ge₂Sb₂Te₅ layer from oxidation^{36,37} and interlayer diffusion³⁸. The diameter of the VO₂ NPs and the thickness of GST were optimized by the aforementioned finite-difference time-domain simulations. Finally, the GST layer of 90 nm was sputtered and the VO₂ NPs with the radius of 45 nm were spin coated from a colloidal solution. The VO₂ NPs size was confirmed by transmission electron microscopy. Ab image of the particles is presented in Fig. 1b.

The reversible phase transitions of the VO₂ NPs and GST are accompanied by a reversible change to the optical properties. As shown in Fig. 1c, the monoclinic state of the VO₂ NPs displays a distorted structure with zigzag-type V–V atomic chains at room temperature and it changes to tetragonal state with straight V–V chains above ~65 °C. This change in structure causes the optical properties to change as evident by the refractive index shown in Fig. 1e. Similarly, Fig. 1d shows how the amorphous structure of Ge₂Sb₂Te₅ crystallizes into to face centered cubic (FCC) structure above 180 °C. Again, this phase transition is accompanied by an abrupt change to the refractive index, see Fig. 1f. Note, the re-amorphous state of Ge₂Sb₂Te₅ is achieved by quenching the material from a temperature above the melting temperature ($T_M = 873$ K). This is possible by laser or electrical pulses.

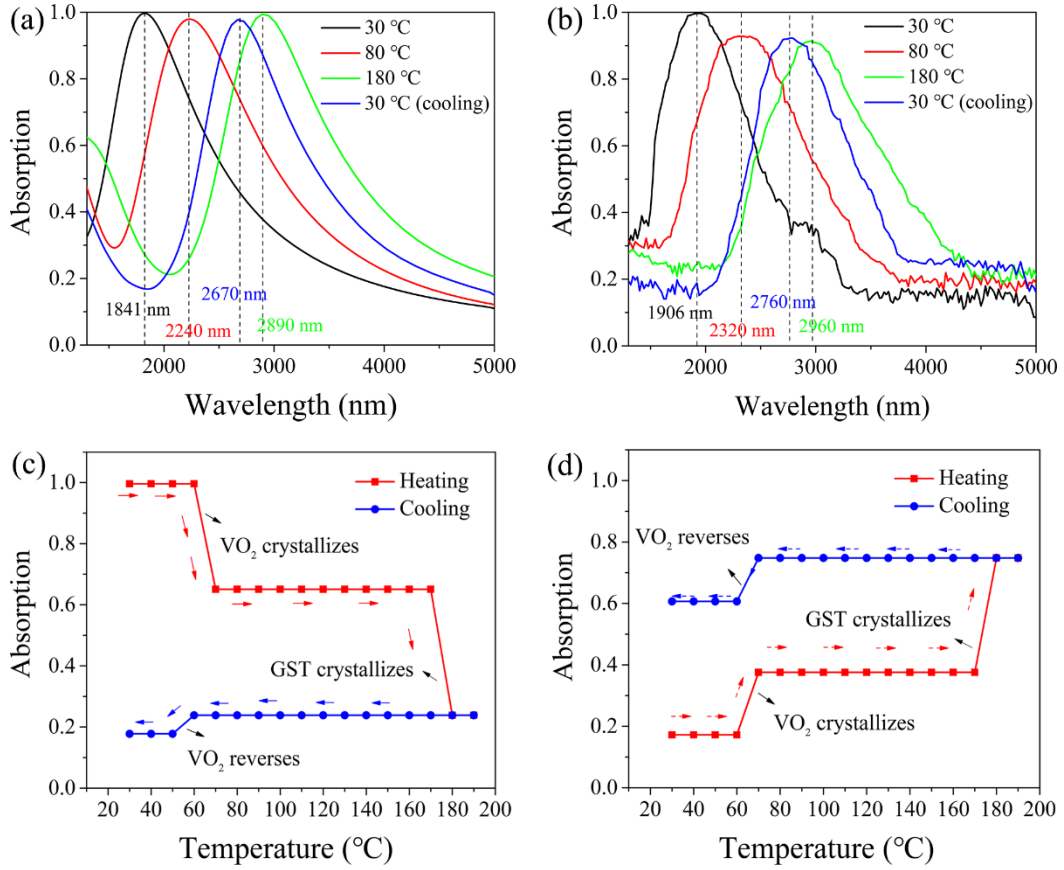


Figure 2 (a) Simulated and (b) measured absorption changes with wavelength ω under 30 °C, 80 °C, 180 °C, and cooling back to 30 °C. The measured absorption changes with temperature at the wavelength of (c) 1900 nm and (d) 3300 nm.

Fig. 2 shows the simulated and measured absorption of the proposed structure. The absorption ($A(\lambda)$) is derived from $A(\lambda) = 1 - T(\lambda) - R(\lambda)$. Since the transmittance spectrum ($T(\lambda)$) for the proposed absorber is zero, $A(\omega) = 1 - R(\lambda)$, where $R(\lambda)$ is the reflectance spectrum of the absorber. The simulated absorption of the metasurface is presented in Fig. 2a. At room temperature, an absorption peak with $A(\lambda_1=1841 \text{ nm}) = 0.99$ is achieved with the amorphous $\text{Ge}_2\text{Sb}_2\text{Te}_5$ layer and monoclinic VO_2 NPs. When temperature is raised to 80 °C, the resonant peak spectrally redshifts to $\lambda_2 = 2240 \text{ nm}$ while maintaining a high absorptance peak of $A(\lambda_2 = 2240 \text{ nm}) = 0.97$. On this state, the GST layer is still amorphous and the VO_2 NPs turn into tetragonal state. Then continuing to increase the temperature to 180 °C causes the resonant peak to spectrally redshifted

to $\lambda_3 = 2890$ nm with the $A(\lambda_3 = 2890 \text{ nm}) = 0.99$ due to the crystallization of $\text{Ge}_2\text{Sb}_2\text{Te}_5$ layer. Now, decreasing the temperature to 30 °C, causes the resonant peak to blueshift to $\lambda_4 = 2670$ nm with the $A(\lambda_4 = 2670 \text{ nm}) = 0.97$. The simulated results show nearly perfect absorption for all four possible states of the device. Moreover, the resonant wavelengths can be tuned across a broad 1000 nm spectral band.

The measured absorption spectrum of the device is presented in Fig. 2b. The $A(\lambda) > 0.9$ for all four possible states of the device, and as per the simulated spectra, the absorption peaks can be programmed across a broad 1000 nm band using heat stimuli. The slight difference between the simulation and measurements is likely due to surface roughness and fabrication imperfections, which were included in the simulation. Nonetheless, the main features of the simulation agree with the measurement, and this validates trustworthiness of our design approach.

From the measured spectrum, we can also see that the device can be used as an IR multi-level switch for a fixed wavelength of light. As examples Figs. 2c and 2d show $A(\lambda=1900)$ and $A(\lambda=3300 \text{ nm})$ as a function of temperature. With temperature changes, $A(\lambda)$ changes 80% and 60% at the wavelength of 1900 nm and 3300 nm, respectively. The large absorption contrast is beneficial for the active tunable photonics devices.

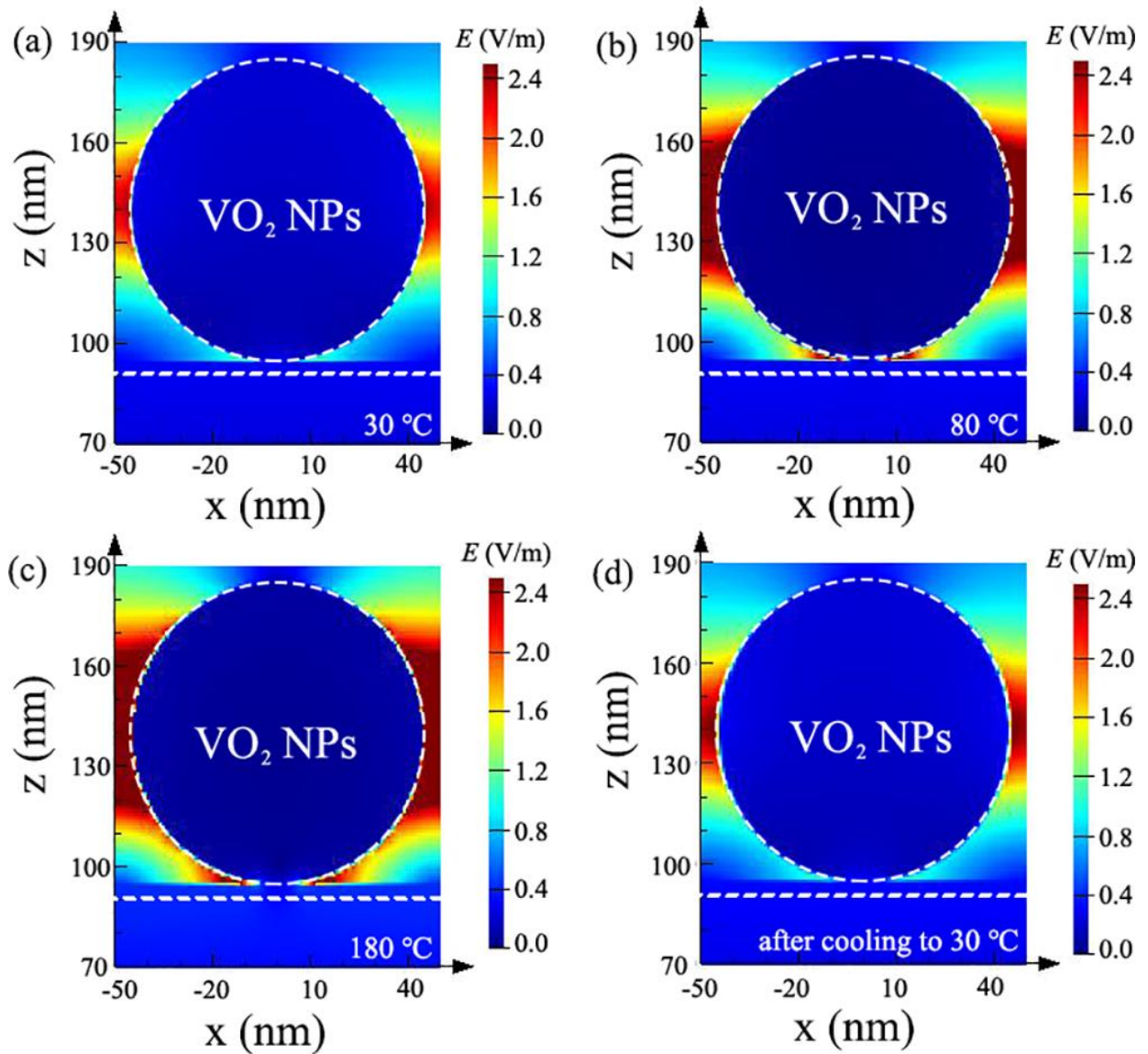


Figure 3 E-field intensity at the resonant wavelength along the cross-section plane for the phase-change metasurfaces at the absorption peak at different temperature: (a) 30 °C; (b) 60 °C; (c) 180 °C; (d) after cooling back to 30 °C.

We have demonstrated 4-wavelength spectral tunability and nearly perfect absorption using our Ge₂Sb₂Te₅-VO₂ metasurface. We have also simulated the spectral response using the FDTD method to numerically solve Maxwell's equations. Since the simulated spectrum essentially agrees with the measured spectrum, we can trust that FDTD models can be used to explore the underlying physics of the structure. The VO₂ NPs (tetragonal state) produce electric dipolar and the strong magnetic resonances between the Au layer and VO₂ NPs. These resonances depend on the state and concomitant permittivity of the

VO₂ NPs and the Ge₂Sb₂Te₅ layer. To understand how the LSPRs and the phase transition of these materials effect the resonant modes, total electrical (E-) field distribution ($E = \sqrt{|E_x|^2 + |E_y|^2 + |E_z|^2}$) for the different resonant wavelength was studied. The total E-fied distribution is presented in Fig. 3. At room temperature and at $\lambda_1 = 1841$ nm Fig. 3a shows that the E-field between the monoclinic VO₂ NPs is weak. Fig. 3b shows the E-field distribution at $\lambda_2 = 2240$ nm when the temperature is above 80 °C. At this state, strong electrical resonances were produced in the gap between the tetragonal VO₂ NPs and the substrate. However, compared with crystalline Ge₂Sb₂Te₅ layer (Fig. 3c), the amorphous Ge₂Sb₂Te₅ layer decreases the plasmonic resonance between the VO₂ NPs and the Au layer. As shown in Fig. 3c, a strong E-field appears not only in the gap of the VO₂ NPs, but also at the bottom side of NP when $\lambda_3 = 2890$ nm and the temperature increase above 180 °C. At this temperature, the VO₂ NPs are in tetragonal state and the GST layer is in its higher refractive index FCC state. Plasmonic resonances are now easily produced between the VO₂ NPs and the Au layer. When the temperature cools to room temperature, the E-field distribution the absorption peak shifts to a wavelength of $\lambda_4 = 2670$ nm, as seen in Fig. 3d. At this temperature, the VO₂ NPs switch into the insulator state yet the Ge₂Sb₂Te₅ remains in the FCC state. Now, it is hard to see any plasmonic effects for the monoclinic VO₂ NPs. These field simulation shows how the states changes the Ge₂Sb₂Te₅ layer and the VO₂ NPs produce different distributions plasmonic fields, this enabling tuning of the resonant wavelengths and modes.

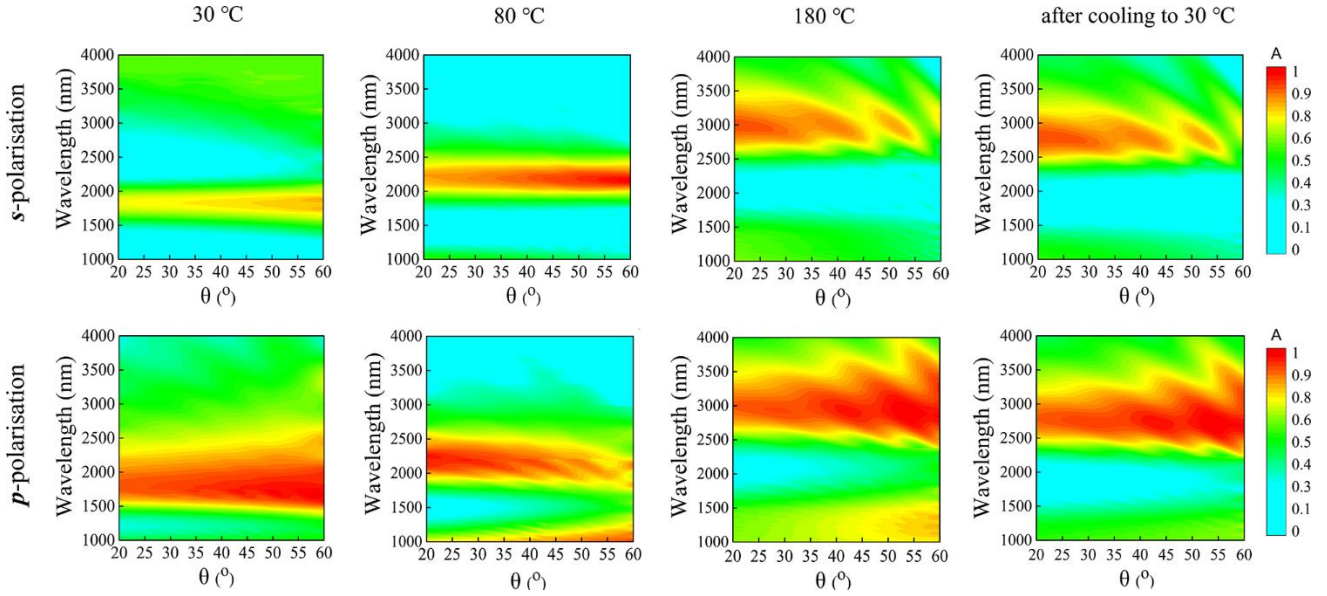


Figure 4 Angular-dependent absorbance spectra at different temperature under the illumination of (a) p-polarization; (b)s- polarization

The proposed metasurface is omnidirectional and polarization independent across a broad range of incident angles. This is a key factor for ideal emitters, photo detectors, and thermal photovoltaics. Fig. 4 shows the $A(\lambda)$ spectra as the function of incident angle (θ) for p- and s- polarization states. These absorption measurements were measured for the four states of the device. For all possible structural states of the phase change materials and for all the measured angles of incidence, we can see that the absorption is greater than 80% and 90% for the s- and p-polarization states respectively. Between the p- and s-polarized light, the $A(\omega)$ peaks exhibit a good spectral overlap for all the four levels.

In summary, we have designed, simulated, and characterized a prototype 4-level reprogrammable near-perfect absorber that exploits the tunable refractive indices of VO_2 NPs and $\text{Ge}_2\text{Sb}_2\text{Te}_5$ thin films. The absorber was fabricated using an efficient low cost and lithography-free method. We theoretically and experimentally demonstrated that the

peak absorption wavelengths of this perfect absorber could be tuned across a broad wavelength band ranging from 1900 to 2900 nm with the $A(\omega) > 90\%$. The absorption seems to be insensitive to the polarization state and the angle of incidence. These attributes are attractive for tunable-wavelength omnidirectional emitters and detectors.

Acknowledgements

This work was supported by National Research Foundation, Prime Minister's Office, Singapore under its Campus for Research Excellence and Technological Enterprise (CREATE) program and Singapore Ministry of Education (MOE) Academic Research Fund Tier 1 RG103/19 and RG86/20. RES acknowledges support the support granted for the Nanospatial Light Modulators for Next-Gen Display Technologies (NSLM) project (A-Star AME grant number: A18A7b0058).

Data Availability

The data that support the findings of this study are available from the corresponding author upon reasonable request.

References

- ¹ H. Yu, K. Lee, J. Park, and Y. Park, *Nat. Photonics* **11** (3), 186 (2017).
- ² Z. Wang, Z. Tong, Q. Ye, H. Hu, X. Nie, C. Yan, W. Shang, C. Song, J. Wu, and J. Wang, *Nat. Commun.* **8** (1), 1 (2017).
- ³ D. Fan, T. Burger, S. McSherry, B. Lee, A. Lenert, and S. R. Forrest, *Nature* **586** (7828), 237 (2020).
- ⁴ C. Li, W. Zhu, Z. Liu, S. Yan, R. Pan, S. Du, J. Li, and C. Gu, *Appl. Phys. Lett.* **113** (23), 231103 (2018).
- ⁵ K. V. Sreekanth, S. Han, and R. Singh, *Adv. Mater.* **30** (21), 1706696 (2018).
- ⁶ A. K. U. Michel, S. Meyer, N. Essing, N. Lassaline, C. R. Lightner, S. Bisig, D. J. Norris, and D. N. Chigrin, *Adv. Opt. Mater.* **9** (2), 2001243 (2021).
- ⁷ Z. Zhu, P. G. Evans, R. F. Haglund Jr, and J. G. Valentine, *Nano Letters* **17** (8), 4881 (2017).
- ⁸ Y. Meng, T. Cao, and Y. Long, *J. Appl. Phys.* **128** (14), 140904 (2020).
- ⁹ T. Cao, K. Liu, L. Lu, J. Liu, Y. J. Liu, K. R. Qin, H. C. Chui, and R. E. Simpson, *Adv. Opt. Mater.* **8** (6), 1901570 (2020).

10 L. Long, S. Taylor, X. Ying, and L. Wang, *Mater. Today Energy* **13**, 214 (2019).
11 A. Tittl, A. K. U. Michel, M. Schäferling, X. Yin, B. Gholipour, L. Cui, M. Wuttig, T. Taubner,
F. Neubrech, and H. Giessen, *Adv. Mater.* **27** (31), 4597 (2015).
12 X. Lu, J. Y. Lee, and Q. Lin, *Appl. Phys. Lett.* **116** (22), 221104 (2020).
13 Y. Jiang, M. Zhang, X. Duan, H. Zhang, and W. Pang, *Appl. Phys. Lett.* **111** (2), 023505 (2017).
14 T. Cao, C.-W. Wei, L.-B. Mao, and S. Wang, *Opt. Express* **23** (14), 18620 (2015).
15 Z. Fang, Y. Wang, A. E. Schlather, Z. Liu, P. M. Ajayan, F. J. García de Abajo, P. Nordlander,
X. Zhu, and N. J. Halas, *Nano Letters* **14** (1), 299 (2014).
16 D. Shrekenhamer, W.-C. Chen, and W. J. Padilla, *Phys. Rev. Lett.* **110** (17), 177403 (2013).
17 M. Wuttig and N. Yamada, *Nat. Mater.* **6** (11), 824 (2007).
18 J. K. Behera, X. Zhou, J. Tominaga, and R. E. Simpson, *Opt. Mater. Express* **7** (10), 3741 (2017).
19 P. Li, X. Yang, T. W. Maß, J. Hanss, M. Lewin, A.-K. U. Michel, M. Wuttig, and T. Taubner,
Nat. Mater. **15** (8), 870 (2016).
20 M. Rudé, R. E. Simpson, R. Quidant, V. Pruneri, and J. Renger, *ACS Photonics* **2** (6), 669
(2015).
21 T. Cao, R. Wang, R. E. Simpson, and G. Li, *Prog. Quantum Electron.*, 100299 (2020).
22 R. Soma, B. Nakayama, M. Kuwahara, E. Yamamoto, and T. Saiki, *Appl. Phys. Lett.* **117** (22),
221601 (2020).
23 Y. Meng, J. K. Behera, S. Wang, M. Jiang, J. Lin, J. Wei, Y. Wang, T. Cao, and Y. Long, *ACS*
Appl. Mater. Interfaces **12** (26), 29953 (2020).
24 Y. Meng, J. K. Behera, S. Wen, R. E. Simpson, J. Shi, L. Wu, Z. Song, J. Wei, and Y. Wang,
Adv. Opt. Mater. **6** (17), 1800360 (2018).
25 W. Dong, Y. Qiu, X. Zhou, A. Banas, K. Banas, M. B. Breese, T. Cao, and R. E. Simpson, *Adv.*
Opt. Mater. **6** (14), 1701346 (2018).
26 E. Hutter and J. H. Fendler, *Adv. Mater.* **16** (19), 1685 (2004).
27 C. Hägglund, G. Zeltzer, R. Ruiz, I. Thomann, H.-B.-R. Lee, M. L. Brongersma, and S. F. Bent,
Nano Letters **13** (7), 3352 (2013).
28 N. Mou, X. Liu, T. Wei, H. Dong, Q. He, L. Zhou, Y. Zhang, L. Zhang, and S. Sun, *Nanoscale*
12 (9), 5374 (2020).
29 T. Cao, K. Liu, L. Lu, H.-C. Chui, and R. E. Simpson, *Nanoscale* **11** (43), 20546 (2019).
30 Y. Meng, J. K. Behera, Y. Ke, L. Chew, Y. Wang, Y. Long, and R. E. Simpson, *Appl. Phys. Lett.*
113 (7), 071901 (2018).
31 Y. Ke, Q. Zhang, T. Wang, S. Wang, N. Li, G. Lin, X. Liu, Z. Dai, J. Yan, and J. Yin, *Nano*
Energy **73**, 104785 (2020).
32 Y. Ke, X. Wen, D. Zhao, R. Che, Q. Xiong, and Y. Long, *ACS Nano* **11** (7), 7542 (2017).
33 N. Wang, Y. K. Peh, S. Magdassi, and Y. Long, *J. Colloid Interface Sci.* **512**, 529 (2018).
34 Y. Ke, B. Zhang, T. Wang, Y. Zhong, T. D. Vu, S. Wang, Y. Liu, S. Magdassi, X. Ye, and D.
Zhao, *Mater. Horiz.* (2021).
35 P. B. Johnson and R. W. Christy, *Phys. Rev. B* **6** (12), 4370 (1972).
36 X. Zhou, W. Dong, H. Zhang, and R. E. Simpson, *Sci. Rep.* **5** (1), 11150 (2015).
37 X. Zhou, Y. Du, J. K. Behera, L. Wu, Z. Song, and R. E. Simpson, *ACS Appl. Mater. Interfaces*
8 (31), 20185 (2016).
38 L. Lu, W. Dong, J. K. Behera, L. Chew, and R. E. Simpson, *J. Mater. Sci.* **54** (4), 2814 (2019).